

# Split-Mode Evidence for No Ultraslow Component to the Source of the 2010 Maule, Chile, Earthquake

by Emile A. Okal, Sutatcha Hongsresawat,\* and Seth Stein

**Abstract** We present a comprehensive study of the Earth's gravest spheroidal modes excited by the Maule, Chile, earthquake of 27 February 2010, using uninterrupted time series extending over a minimum of 19 and a maximum of 93 days. For each of 101 station-mode combinations, we use the formalism of [Stein and Geller \(1977\)](#) to compute the relative excitation of the  $2l + 1$  singlets in the relevant geometry and obtain an estimate of the seismic moment by best fitting the observed spectrum to that of the resulting synthetic computed for the same recording window. The average results for seven spheroidal and two radial modes deviate no more than 12% from the Global Centroid Moment Tensor moment of  $1.86 \times 10^{29}$  dyn·cm, with no evident trend with frequency. In other words, we fail to document an ultralow-frequency component (expressed as an increase of moment with period) in the source of the 2010 event. This result indicates that such components are not universal features of megaquakes, even though they had been documented for the 1960 Chilean, 2004 Sumatran, and 1964 Alaskan events (the only three events with larger moments in the past 50 years). In this respect, the 2010 earthquake is most comparable to the slightly smaller 2005 Nias event, which incidentally also featured a bilateral rupture.

## Introduction

A remarkable aspect of the great 2004 Sumatra-Andaman earthquake was the slowness of its source. Although its Centroid Moment Tensor (CMT) solution featured a seismic moment of only  $3.95 \times 10^{29}$  dyn·cm (even computed at a period of 300 s, rather than at the customary 135 s), the more definitive value of 1 to  $1.2 \times 10^{30}$  dyn·cm ([Stein and Okal, 2005](#); [Tsai et al., 2005](#)) was 2.5–3 times larger. Figure 1 shows that, for all but the gravest modes, the moments computed from the modeling of the Earth's normal modes increase systematically with their periods, due to the destructive interference in the source spectrum resulting from a slow source. Based on the analysis of the gravest toroidal modes (and in particular of  ${}_0T_2$ , which had not been previously observed), [Park et al. \(2008\)](#) have suggested that the source of the Sumatra earthquake may have been even slower than that of the composite model of [Tsai et al. \(2005\)](#), which lasted 600 s. In addition, source tomography studies, using beam-forming techniques on body waves and hydroacoustic ( $T$ ) waves ([deGroot-Hedlin, 2005](#); [Guilbert et al., 2005](#); [Ishii et al., 2005](#); [Krüger and Ohmberger, 2005](#); [Tolstoy and Bohnenstiehl, 2005](#)), resolved rupture velocities along the fault on the order of 2.5–2.8 km/s, which is significantly less than the average value of 3.5 km/s expected from earthquake

scaling laws, although such velocities remain much higher than those typical of the so-called tsunami earthquakes, such as the 1992 Nicaragua and 1994 and 2006 Java events. Finally, the Sumatra-Andaman earthquake featured a deficient energy-to-moment ratio ([Choy and Boatwright, 2007](#)), expressed as  $\Theta = -5.98$  in the formalism of [Newman and Okal \(1998\)](#), a value typical of slow sources such as tsunami earthquakes.

The largest earthquake ever recorded, the 1960 Chilean event, has long been known to have featured an extremely slow component to its source ([Kanamori and Cipar, 1974](#); [Kanamori and Anderson, 1975](#); [Cifuentes and Silver, 1989](#)). The moment of the second largest event, the 1964 Alaskan earthquake, computed as  $M_0 = 8.5 \times 10^{29}$  dyn·cm from 200-s surface waves ([Kanamori, 1970](#)), was later reevaluated by [Nettles et al. \(2005\)](#) using much longer periods (up to 600 s) and found to be at  $1.3 \times 10^{30}$  dyn·cm. This shows that the Alaskan earthquake, too, features slowness in its source.

Thus, the three largest events ever recorded are characterized by a slow source, and this observation raises the legitimate question of whether all megaquakes (which can be broadly defined as having  $M_0 > 10^{29}$  dyn·cm) share this property, even though [Stein and Okal \(2007\)](#) showed that the 2005 Nias earthquake (at the time the sixth largest) does not. The occurrence of the Maule, Chile, earthquake of 27 February 2010 ( $M_0 = 1.86 \times 10^{29}$  dyn·cm) provides an

\*Present address: Department of Geological Sciences, University of Florida, Gainesville, Florida 32611.

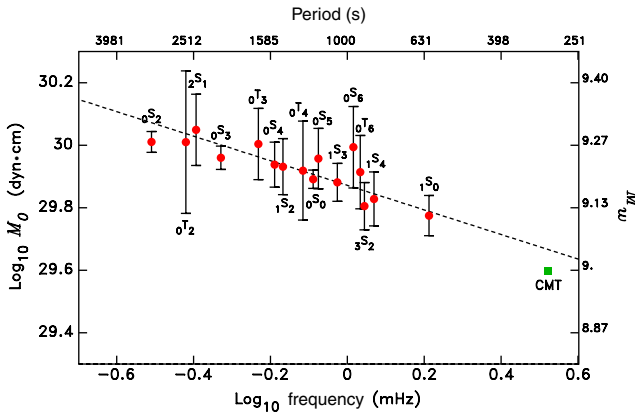


**Figure 1.** Evidence of source slowness of the 2004 Sumatra-Andaman earthquake showing seismic moment retrieved from the spectra of the Earth's normal modes. Note the systematic increase of  $M_0$  with period (after Okal and Stein, 2009). The color version of this figure is available only in the electronic edition.

opportunity to explore this question further. We conclude that the Maule event does not feature a detectable slow component to its source spectrum.

#### Methodology and Theoretical Background

In the weeks following the 2010 Maule event, we gathered high-quality time series of its records at stations of the global networks (Incorporated Research Institutions for Seismology [IRIS], GEOSCOPE, and GEOFON) and modeled their spectra as described by Okal and Stein (2009). We targeted the gravest modes of the Earth,  ${}_0S_2$  to  ${}_0S_5$  and  ${}_1S_2$  to  ${}_1S_4$ , as well as the two radial modes  ${}_0S_0$  and  ${}_1S_0$ . We do not consider toroidal modes, because their generally lower  $Q$  values lead to records of poorer quality. The mode  ${}_1S_3$  was combined with  ${}_3S_1$ , which has a similar frequency, and their singlets were processed as a single multiplet for the purpose of the analysis.

As discussed by Dahlen (1982), an optimal spectrum of a free oscillation of the Earth requires a record with a duration on the order of half the product of its period  $T$  by its quality factor  $Q$ . Any shorter window will not adequately resolve the shape of the spectral line, while a significantly longer window will include excessive noise that occurs after the decay of the oscillation. Split modes require longer time windows to fully reflect their beating pattern. For the modes targeted in this study, which feature  $T = 1000\text{--}3000$  s and  $Q = 300\text{--}550$ , a two- to three-week window is usually adequate, with the exception of  ${}_0S_0$ , which requires a window of 90 days because of its exceptionally high  $Q$ . Finally, we used only stations with no gap in the recording, which strongly limited the final dataset.

For each record and each targeted  ${}_nS_l$ , we Fourier transformed an adequate time window (varying from 2 to 13 weeks and starting one hour after the origin time) and removed the instrument response to obtain the observed spectral amplitude of ground motion  $X_{\text{obs}}(\omega)$ . The example

in Figure 2 illustrates the splitting of the modes, a property first documented by Benioff *et al.* (1961) (and hinted at by Ness *et al.*, 1961) during the first observations of the Earth's free oscillations following the 1960 Chilean earthquake.

We recall that the free oscillations of a spherical non-rotating laterally homogeneous Earth are degenerate with respect to the azimuthal order  $m$ ; that is, that their (angular) eigenfrequencies  $({}_n\omega)_{\text{SNRH}}$  should not depend on  $m$ . However, rotation and ellipticity (as well as lateral heterogeneity) lift the degeneracy, splitting the multiplet  ${}_nS_l$  into  $2l + 1$  singlets with slightly different eigenfrequencies  ${}_n\omega_l^m$ . Pekeris *et al.* (1961), Backus and Gilbert (1961), and Dahlen (1968) gave expressions for the frequency shifts  ${}_n\omega_l^m - ({}_n\omega)_{\text{SNRH}}$ , and an authoritative list of theoretical splitting parameters was later computed by Dahlen and Sailor (1979).

For a given spheroidal mode  ${}_nS_l$ , a point-source double couple excites at most the five singlets  $|m| \leq 2$  in a frame using the epicenter as the pole of the spherical harmonics. However, rotation and ellipticity mandate the use of spherical harmonics centered on the geographic (north) pole of the Earth, in which all  $2l + 1$  singlets are excited. Using the

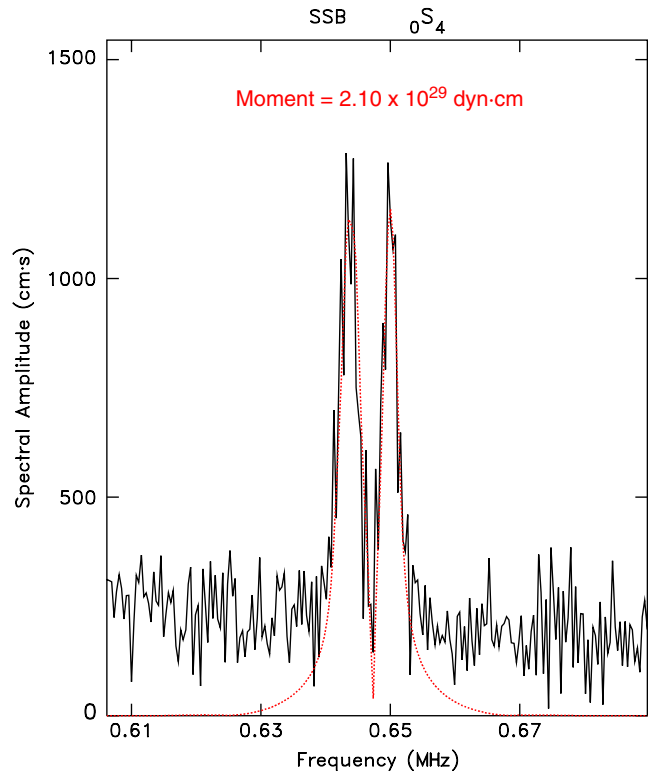


**Figure 2.** Split spectrum of the multiplet  ${}_0S_4$  at the GEOSCOPE station Saint-Sauveur de Badole, France (SSB). The solid trace is the observed spectral amplitude of vertical ground motion  $X_{\text{obs}}(\omega)$ . The time series starts 26 min after the origin time and is 19.5 days long. Although the spectrum features two broad peaks, it is actually composed of nine singlets, widened by anelastic attenuation to the extent that not all can be separated. The dotted line is the synthetic spectrum  $X_{\text{synt}}(\omega)$ . A least-squares fit of the two curves yields the seismic moment at the period of the multiplet,  $2.1 \times 10^{29}$  dyn·cm. The color version of this figure is available only in the electronic edition.

concept of projection of spherical harmonics between those two frames, Stein and Geller (1977) derived excitation coefficients of geographic singlets for any source geometry.

For each station, we use the Global CMT focal mechanism ( $\phi = 8^\circ$ ;  $\delta = 18^\circ$ ;  $\lambda = 116^\circ$ ) and combine these coefficients with the amplitudes of the associated Legendre functions  $Y_l^m$  at the station, to produce a stick plot illustrating the amplitudes of oscillation of all singlets at the relevant receiver (Fig. 3). Because the Coriolis frequency shift is linear in  $m$  but the ellipticity term is quadratic (Dahlen, 1968), the spacing of the singlets with frequency can be irregular, and this occasionally leads to their pattern being wrapped around, with, for example,  ${}_n\omega_l^l < {}_n\omega_l^{l-1}$ .

The stick plots are then used to build synthetic seismograms of the multiplet by simply combining the  $2l + 1$  singlets (each oscillating with the appropriate amplitude and at its own frequency) into a beating pattern. These computations are carried out in the time domain for precisely the same time window as in the observed seismogram. They use a reference unit scalar moment and the  $Q$  values published for each multiplet by Widmer *et al.* (1991). The theoretical seismogram includes the response of the instrument, which is sensitive not only to the ground acceleration but also to the induced change in gravity potential and to the tilt resulting from the finite wavelength of the oscillation. These terms, detailed by Gilbert (1980), are included in our synthetic record.

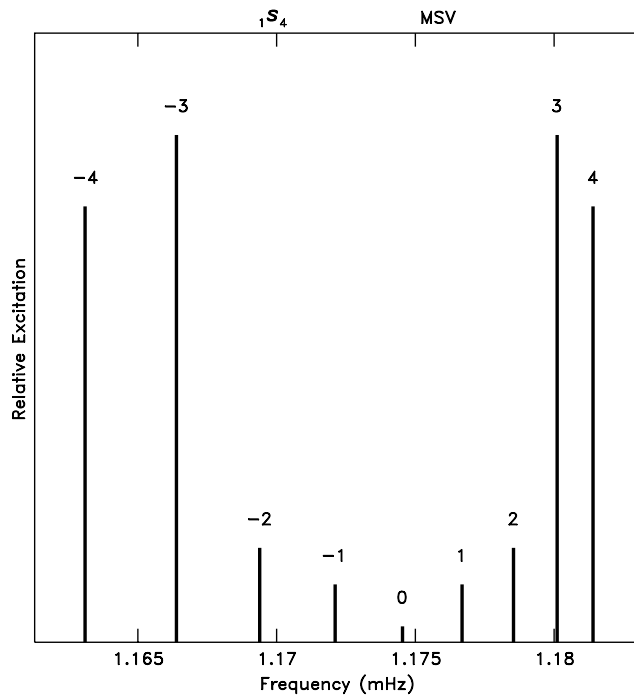


**Figure 3.** Example of stick plot for the multiplet  ${}^1S_4$  at Monasavu, Fiji. For each of the nine singlets ( $-4 \leq m \leq 4$ ), the height of the vertical bar illustrates the combined amplitudes of the excitation of the singlet by the source and of the amplitude of  $Y_l^m$  at the station. Note the nonlinearity of the frequency shifts with  $m$ .

The latter is then processed with the same fast-Fourier transform algorithm as the data, and a theoretical spectral amplitude  $X_{\text{synt}}(\omega)$  is derived. The ratios  $X_{\text{obs}}/X_{\text{synt}}$  are best fit inside a narrow frequency band to obtain an estimate of the moment  $M_0$  of the source at the frequency  ${}_n\omega_l$ . Figure 4 gives examples of the fitting of the spectral lines for each of the modes targeted. In the case of the combination of  ${}^1S_3$  and  ${}^3S_1$ , the proper excitation coefficients (derived from the respective eigenfunctions) and  $Q$  values were used for each multiplet, but the 10 singlets were then regrouped into a single set for the purpose of determining a moment value by least-squares fitting of the observed windowed spectrum.

The procedure is slightly different in the case of the radial modes  ${}_0S_0$  and  ${}_1S_0$ , which are obviously not split, and for which we used  $Q = 5579$  and 2017, respectively, as determined by Okal and Stein (2009). For  ${}_0S_0$ , we were able to find only six continuous records with durations between 71 and 93 days. Results are shown in Figure 5.

The moment values obtained in this study obviously rely on an adequate knowledge of instrument gains, for which the accuracy was estimated by Davis *et al.* (2005) as no better than 15% on the average and 25% in a few cases. While acknowledging this source of potential error in our results, we emphasize that the moments of the various modes were generally obtained from records at the same group of stations, reducing any effect on the relative values of the moments extracted from different modes. Furthermore, the error on  $M_0$  would be expected to be no more than 15%, or 0.04 units of moment magnitude (Kanamori, 1977), while we seek to document a source slowness comparable to that of the Sumatra event, involving a factor of 3 between the CMT frequencies and the gravest modes. Similarly, Zürn and Widmer (1995) have documented that correcting for the effect of meteorological pressure variations on the seismic sensor could greatly improve the signal-to-noise ratio of the gravest modes during the 1994 Kuriles and Bolivia earthquakes. However, this effect is going to become irrelevant for the Maule earthquake, for which the moment is six times larger and for which our selected spectral lines, as presented in Figure 5, are clearly pulled out of the noise.

## Results and Discussion

We obtained a total of 101 measurements of the seismic moment of the 2010 Maule earthquake, at periods ranging from 613 to 3233 s. For each mode, we present in Table 1 the best-fitting seismic moment, geometrically averaged over all stations. Standard deviations are expressed as a multiplicative or divisive factor ( $\times/$ ) about each average value.

The dataset, plotted in Figure 6, shows no detectable trend of  $M_0$  versus frequency, contrary to the case of the 2004 Sumatra–Andaman earthquake. This is confirmed by the fact that the moment averaged over the full dataset of 101 values,  $M_0 = 1.87 \times 10^{29} \text{ dyn}\cdot\text{cm} (\times/1.06)$ , is indistinguishable from the CMT value of  $1.86 \times 10^{29} \text{ dyn}\cdot\text{cm}$ . In contrast, the 2004 Sumatra event featured a regular

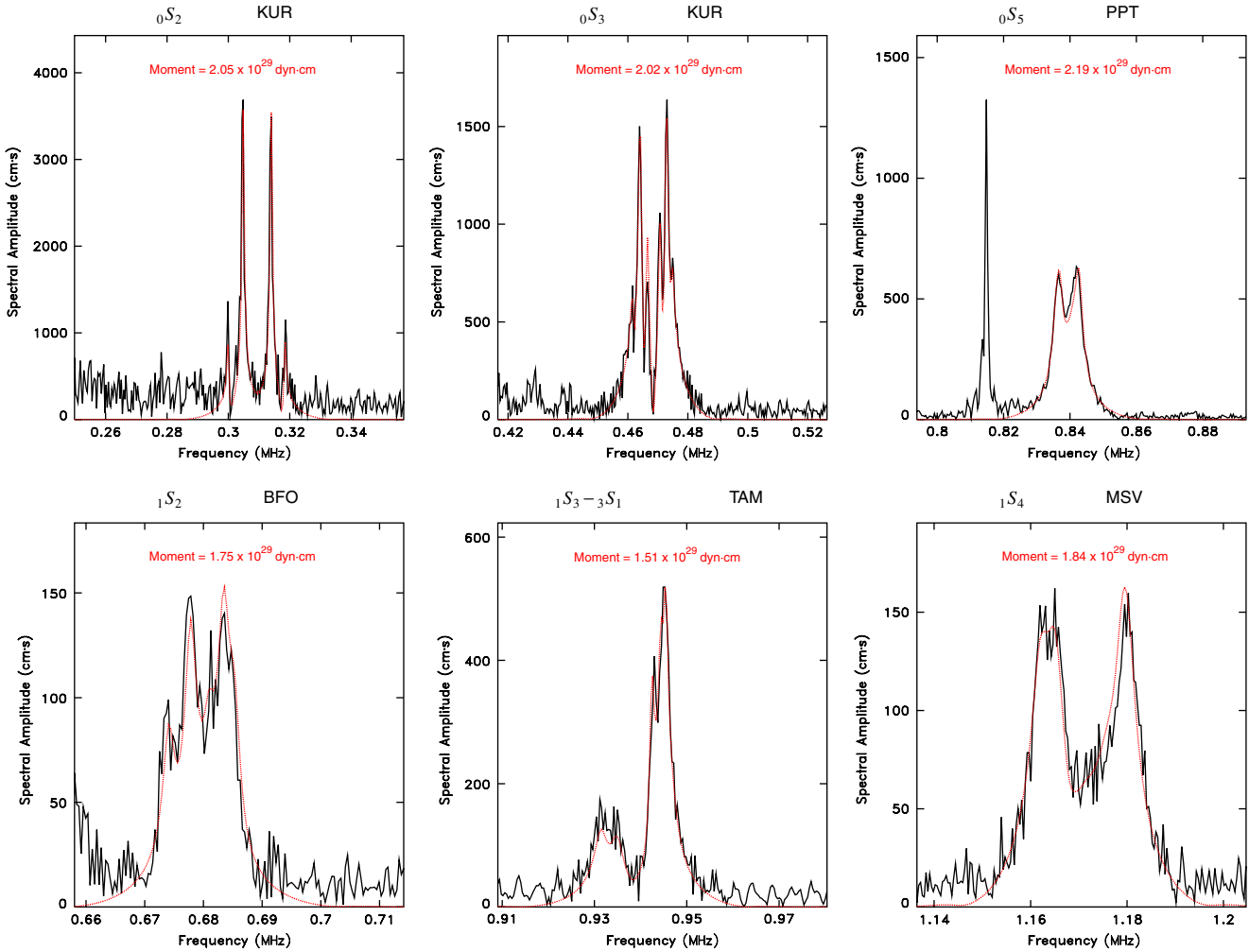


**Figure 4.** Same as Figure 2 for the other spheroidal modes at five additional stations. For each multiplet, results are given at a representative station. In the case of  ${}_0S_5$ , the spectral line at the left is the radial mode  ${}_0S_0$ , which is outside the window used for least-squares modeling. In the case of  ${}_1S_3 - {}_3S_1$ , the dominant narrow singlets are those of the higher overtone  ${}_3S_1$  (which penetrates the core), while the broader, more attenuated singlets at the left belong to  ${}_1S_3$  (which is more concentrated in the mantle). The color version of this figure is available only in the electronic edition.

increase of moment with period, with a logarithmic slope of 0.39 in the range of frequencies considered (dashed line in Fig. 1). In the same logarithmic units, a weighted regression through the 2010 dataset yields a slope of  $-0.002$ , which is not significantly different from 0. Clearly, the 2010 spectrum plotted in Figure 6 is flat.

The bottom line of this study is that the 2010 data, processed with the exact same algorithm as used for the 2004 Sumatra and 2005 Nias earthquakes (admittedly including the same limitations regarding the effects of imprecise gains, barometric noise, etc.), fail to unravel the kind of frequency dependence of the seismic moment that characterized the source of the 2004 Sumatra event as slow.

This result is also in agreement with the energy-to-moment ratio computed for the Maule earthquake, in the formalism of Newman and Okal (1998), which yields a parameter  $\Theta = \log_{10}(E^E/M_0) = -5.35$ . This value is characteristic of subduction environments, as shown in Figure 7.

By contrast, the 2004 Sumatra–Andaman earthquake featured  $\Theta = -5.98$ , comparable to other slow sources, such as the 1992 Nicaragua, 1996 Chimbote, Peru, and 1994 and 2006 Java earthquakes (Choy and Boatwright, 2007).

Our results would seem to contradict the recent study by Tanimoto and Ji (2010), who have proposed that the excitation of  ${}_0S_2$  and  ${}_0S_3$  may be 10%–20% greater than that predicted from the CMT solution, which they interpret as the occurrence of afterslip. In the case of  ${}_0S_2$ , our average moment is indeed 10% greater than the CMT value, but we would argue that this figure, for which the error bar is itself a factor of 10% (see Table 1) and which corresponds to a difference of only 0.03 units of moment magnitude (Kanamori, 1977), falls within the general precision with which seismic moments are computed, as evidenced by the comparison between values routinely inverted by various agencies, using different datasets and algorithms (National Earthquake Information Center, Global CMT, etc.). We note also that

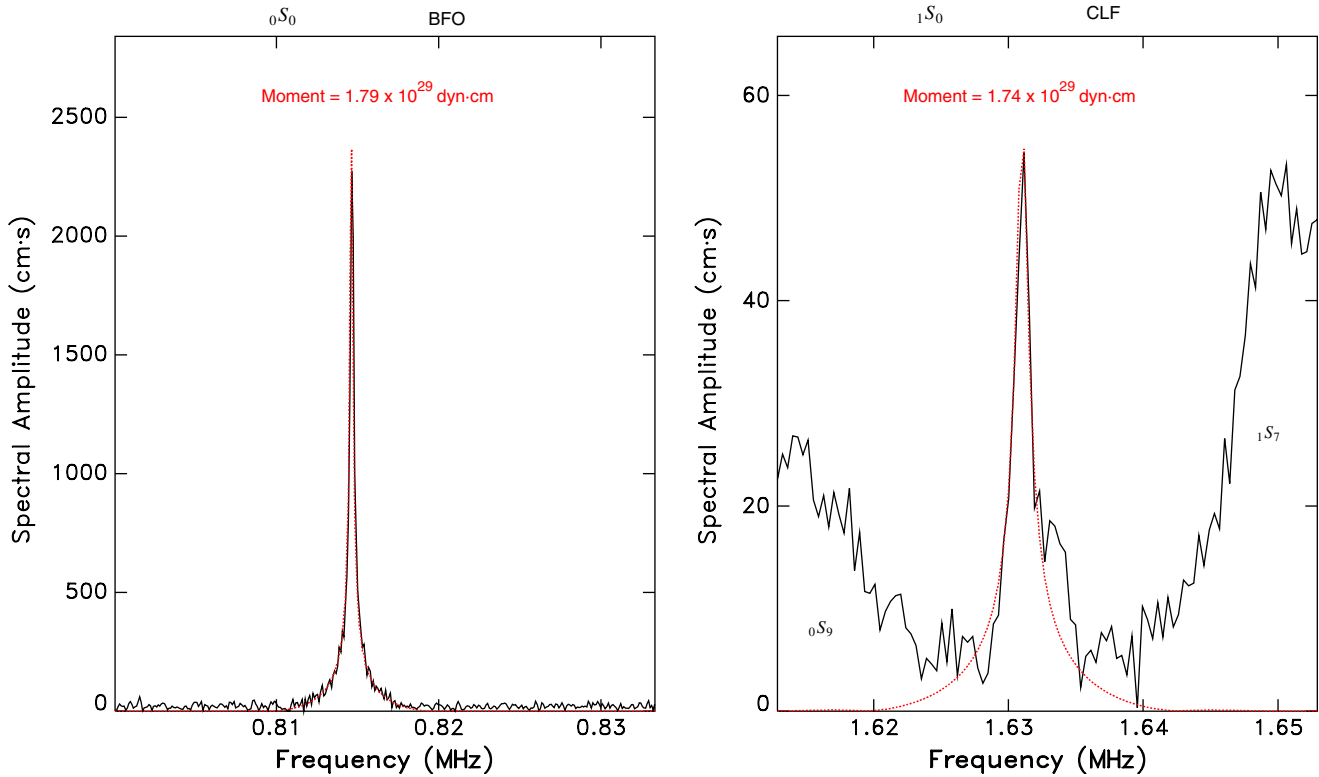


**Figure 5.** Same as Figure 4 for the radial modes  ${}_0S_0$  and  ${}_1S_0$ . For the latter, the broad peaks on either side are the neighboring spheroidal modes  ${}_0S_9$  and  ${}_1S_7$ , which lie outside of the window used for modeling. The color version of this figure is available only in the electronic edition.

Tanimoto and Ji (2010) do not use a full modeling of the excitation of the various singlets of these strongly split modes. Furthermore, their use of short time windows (not exceeding 3 days) undersamples the fine structure of the relevant multiplets and at any rate falls short of the optimal duration of 9 days (for an unsplit mode) proposed by Dahlen (1982). Finally, we reemphasize that our goal in the present study was to explore the possibility of a strong growth of  $M_0$  between the CMT periods and the gravest modes, similar to the factor of 3 evidenced in the 2004 Sumatra event. Neither our study nor, for that matter, the study by Tanimoto and Ji (2010) indicate such a behavior.

Thus, the 2010 Maule event did not feature the source slowness characterizing the three largest earthquakes ever recorded: Chile (1960), Alaska (1964), and Sumatra (2004). In this respect, the Maule earthquake is reminiscent of the Nias event of 28 March 2005 (Stein and Okal, 2007). It is noteworthy that the Nias and Maule sources share a bilateral rupture geometry, the latter determined by the distribution of aftershocks (Barrientos, 2010) and preliminary source tomography (Lay *et al.*, 2010). However, this property was also featured by the 1946 Aleutian tsunami earthquake, for which the rupture was among the slowest measured (López and Okal, 2006).

In conclusion, there does not seem to be any evident correlation between source slowness and size, nor between source slowness and directivity, among the very largest

events surpassing or approaching  $10^{29}$  dyn·cm. In this respect, it does not seem possible to forecast slowness based on simple, readily available parameters such as geographic location (contrast Chile 1960 and 2010 or Sumatra 2004 and Nias 2005) or mere size. Yet, slowness at ultralong periods is of interest, for example, in the context of transoceanic tsunami warning because tsunami excitation is controlled by the value of  $M_0$  at periods (typically 1000–3000 s) inaccessible to real-time seismic analysis, even using the newly-developed *W*-phase inversion (Kanamori and Rivera, 2008).

Table 1  
Best-Fitting Seismic Moments for Nine Modes

Mode	Period (s)	Seismic Moment $M_0$		
		Average ( $10^{29}$ dyn·cm)	Standard Deviation $\times/*$	Number of Stations
${}_0S_2$	3233	2.06	1.10	4
${}_0S_3$	2135	1.83	1.05	12
${}_0S_4$	1546	1.83	1.17	17
${}_0S_5$	1190	1.99	1.09	14
${}_1S_2$	1471	2.08	1.12	6
${}_1S_3 - {}_3S_1$	1061	1.69	1.07	15
${}_1S_4$	853	1.83	1.06	16
${}_0S_0$	1227	1.89	1.10	6
${}_1S_0$	613	1.88	1.06	11

\*Standard deviation is expressed as a multiplicative or divisive factor ( $\times/$ ) about each average value.

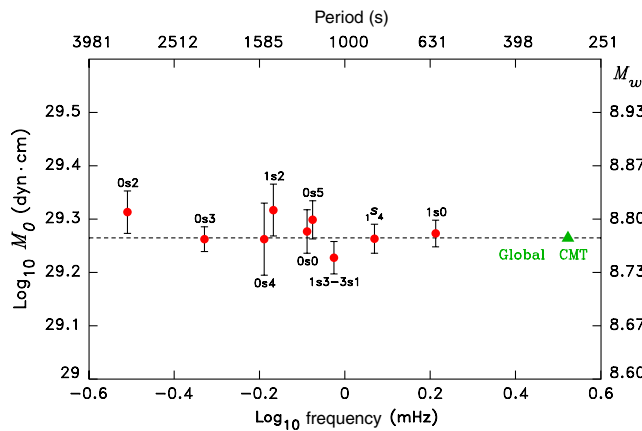


**Figure 6.** Seismic moment of the 2010 Maule earthquake computed from the spectra of its gravest normal modes. For each mode, the average moment is shown as a solid dot, with relevant standard deviation bars. The horizontal dashed line is the Global CMT value. Note the absence of any trend with frequency, contrary to the case of Sumatra shown in Figure 1. The color version of this figure is available only in the electronic edition.

Further work on megaequakes, including historical events for which no definitive ultralong-period solution is available (e.g., Rat Island, 1965; Aleutian, 1957; Kamchatka, 1952) may help shed more light on this challenging question.

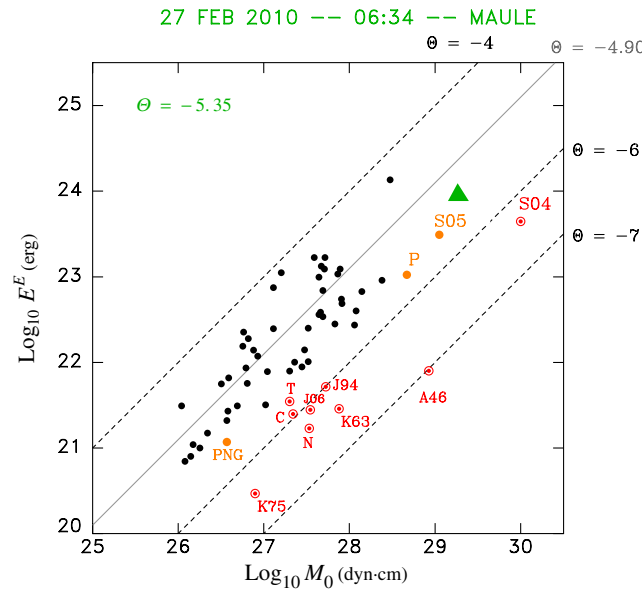


**Figure 7.** Estimated energy  $E^E$  versus seismic moment  $M_0$  for the 2010 Maule event (large triangle) against a backdrop of events adapted from Newman and Okal (1998). Oblique lines feature constant energy-to-moment ratios identified by their parameter  $\Theta$ . Tsunami earthquakes with deficient  $\Theta$  are shown as bull's-eye symbols; N, Nicaragua 1992; T, Tonga, 1982; C, Chimbote, Peru, 1996; J94, Java, 1994; J06, Java, 2006; A46, Aleutian, 1946; K63, Kuriles, 1963; K75, Kuriles, 1975; S04, Sumatra 2004. Also shown for reference are the 1998 Papua New Guinea (PNG), 2001 Peru (P), and 2005 Sumatra Nias (S05) earthquakes. The color version of this figure is available only in the electronic edition.

## Note Added in Proof

Similar results, that is, the total agreement of the amplitude of spheroidal modes with the CMT moment derived at higher frequencies, were also obtained for the 2011 Tohoku earthquake (Okal, 2011).

## Data and Resources

As mentioned in the text, the data were obtained from the Incorporated Research Institutions for Seismology (IRIS), GEOSCOPE, and GEOFON data centers.

## Acknowledgments

The paper benefited from constructive reviews from Jeff Park and another reviewer. We thank Toshiro Tanimoto for discussions during the Fall 2010 meeting of the American Geophysical Union.

## References

- Backus, G., and F. Gilbert (1961). The rotational splitting of the free oscillations of the Earth, *Proc. Natl. Acad. Sci. Unit. States Am.* **47**, 362–371.
- Barrientos, S. (2010). International aftershock response, *Eos, Trans. AGU* **91**, no. 26, Abstract U44B-01.
- Benioff, H., F. Press, and S. Smith (1961). Excitation of the free oscillations of the Earth by earthquakes, *J. Geophys. Res.* **66**, 605–619.
- Choy, G. L., and J. Boatwright (2007). The energy radiated by the 26 December 2004 Sumatra-Andaman earthquake estimated from 10-minute  $P$ -wave windows, *Bull. Seismol. Soc. Am.* **97**, S18–S24.
- Cifuentes, I. L., and P. G. Silver (1989). Low-frequency source characteristics of the great 1960 Chilean earthquake, *J. Geophys. Res.* **94**, 643–663.
- Dahlen, F. A. (1968). The normal modes of a rotating, elliptical Earth, *Geophys. J. Roy. Astron. Soc.* **16**, 329–367.
- Dahlen, F. A. (1982). The effect of data windows on the estimation of free oscillation parameters, *Geophys. J. Roy. Astron. Soc.* **69**, 537–549.
- Dahlen, F. A., and R. V. Sailor (1979). Rotational and elliptical splitting of the free oscillations of the Earth, *Geophys. J. Roy. Astron. Soc.* **58**, 609–623.
- Davis, P., M. Ishii, and T. G. Masters (2005). An assessment of the accuracy of GSN sensor response information, *Seismol. Res. Lett.* **76**, 678–683.
- deGroot-Hedlin, C. D. (2005). Estimation of the rupture length and velocity of the great Sumatra earthquake of Dec. 26, 2004 using hydroacoustic signals, *Geophys. Res. Lett.* **32**, no. 11, L11303, 4 pp.
- Gilbert, F. (1980). An introduction to low-frequency seismology, in *Proceedings of the International School of Physics “Enrico Fermi”*, Course 78, A. M. Dziewoński and E. Boschi (Editors), North Holland, Amsterdam, The Netherlands, 41–81.
- Guilbert, J., J. Vergoz, E. Schisselé, A. Roueff, and Y. Cansi (2005). Use of hydroacoustic and seismic arrays to observe rupture propagation and source extent of the  $M_w = 9.0$  Sumatra earthquake, *Geophys. Res. Lett.* **32**, no. 15, L15310, 5 pp.
- Ishii, M., P. M. Shearer, H. Houston, and J. E. Vidale (2005). Extent, duration and speed of the 2004 Sumatra-Andaman earthquake, imaged by the Hi-net array, *Nature* **435**, 933–936.
- Kanamori, H. (1970). The Alaska earthquake of 1964: Radiation of long-period surface waves and source mechanism, *J. Geophys. Res.* **75**, 5029–5040.
- Kanamori, H. (1977). The energy release in great earthquakes, *J. Geophys. Res.* **82**, 2981–2987.
- Kanamori, H., and D. L. Anderson (1975). Amplitude of the Earth’s free oscillations and long-period characteristics of the earthquake source, *J. Geophys. Res.* **80**, 1075–1078.

- Kanamori, H., and J. J. Cipar (1974). Focal process of the great Chilean earthquake, May 22, 1960, *Phys. Earth Planet. In.* **9**, 128–136.
- Kanamori, H., and L. Rivera (2008). Source inversion of W phase: Speeding up seismic tsunami warning, *Geophys. J. Int.* **175**, 222–238.
- Krüger, F., and M. Ohrnberger (2005). Spatio-temporal source characteristics of the 26 December 2004 Sumatra earthquake as imaged by teleseismic broadband arrays, *Geophys. Res. Lett.* **32**, no. 24, L24312, 4 pp.
- Lay, T., C. J. Ammon, H. Kanamori, K. D. Koper, O. Sufri, and A. R. Hutko (2010). Teleseismic inversion for rupture process of the 27 February 2010 Chile ( $M_w = 8.8$ ) earthquake, *Eos Trans. AGU*, **91**, no. 26, Abstract U44B-02.
- López, A. M., and E. A. Okal (2006). A seismological reassessment of the source of the 1946 Aleutian “tsunami” earthquake, *Geophys. J. Int.* **165**, 835–849.
- Ness, N. F., J. C. Harrison, and L. B. Slichter (1961). Observations of the free oscillations of the Earth, *J. Geophys. Res.*, **66**, 621–629.
- Nettles, M., G. Ekström, A. M. Dziewoński, and N. Maternovskaya (2005). Source characteristics of the great Sumatra earthquake and its aftershocks, *Eos Trans. AGU* **86**, no. 18, Abstract U43A-01.
- Newman, A. V., and E. A. Okal (1998). Teleseismic estimates of radiated seismic energy: The  $E/M_0$  discriminant for tsunami earthquakes, *J. Geophys. Res.* **103**, 26,885–26,898.
- Okal, E. A. (2011). Lessons from Sendai: A perspective from Polynesia and the world, *Geophys. Res. Abstr.* **13**, Abstract EGU2011-14228.
- Okal, E. A., and S. Stein (2009). Observations of ultra-long period normal modes from the 2004 Sumatra-Andaman earthquake, *Phys. Earth Planet. Int.* **175**, 53–62.
- Park, J., A. Amoruso, L. Crescentini, and E. Boschi (2008). Long-period toroidal Earth free oscillations from the great Sumatra-Andaman earthquake observed by paired laser extensometers in Gran Sasso, Italy, *Geophys. J. Intl.* **173**, 887–905.
- Pekeris, C. L., Z. Alterman, and H. Jarosch (1961). Rotational multiplets in the spectrum of the Earth, *Phys. Rev.* **122**, 1692–1700.
- Stein, S., and R. J. Geller (1977). Amplitudes of the Earth’s split normal modes, *J. Phys. Earth* **25**, 117–142.
- Stein, S., and E. A. Okal (2005). Size and speed of the Sumatra earthquake, *Nature* **434**, 581–582.
- Stein, S., and E. A. Okal (2007). Ultra-long period seismic study of the December 2004 Indian Ocean earthquake and implications for regional tectonics and the subduction process, *Bull. Seismol. Soc. Am.* **97**, S279–S295.
- Tanimoto, T., and C. Ji (2010). Afterslip of the 2010 Chilean earthquake, *Geophys. Res. Lett.* **37**, no. 22, L22312, 4 pp.
- Tolstoy, M., and D. R. Bohnenstiehl (2005). Hydroacoustic constraints on the rupture duration, length and speed of the great Sumatra-Andaman earthquake, *Seismol. Res. Lett.* **76**, 419–425.
- Tsai, V. C., M. Nettles, G. Ekström, and A. M. Dziewoński (2005). Multiple CMT source analysis of the 2004 Sumatra earthquake, *Geophys. Res. Lett.* **32**, no. 17, L17304, 5 pp.
- Widmer, R., T. G. Masters, and J. F. Gilbert (1991). Spherically symmetric attenuation within the Earth from normal mode data, *Geophys. J. Int.* **104**, 541–553.
- Zürn, W., and R. Widmer (1995). On noise reduction in vertical seismic records below 2 mHz using local barometric pressure, *Geophys. Res. Lett.* **22**, 3537–3540.

Department of Earth and Planetary Sciences  
Northwestern University  
Evanston, Illinois 60208

Manuscript received 2 September 2010